Direct photon production by positive- and negative-pion beams

A. P. Contogouris, N. Mebarki, H. Tanaka, and S. D. P. Vlassopulos*
Department of Physics, McGill University, Montreal, Canada
(Received 18 April 1985)

Large-p_T direct photon production by $\pi^{\mp}$ beams in the framework of QCD is studied in detail. Higher-order corrections (K factors), photon bremsstrahlung, partons' intrinsic transverse momentum, and higher-twist effects are taken into account. The various ambiguities which beset a theoretical calculation are carefully considered. Comparisons with all available data and further predictions are presented in detail. At fixed energy the ratio of the inclusive cross sections by π^- and π^+ shows a clear increase with p_T. Certain preliminary data do not support this prediction. It is concluded that precise measurements of this ratio offer an important test of QCD.

I. INTRODUCTION

The magnitude of the inclusive cross sections for direct photon production in pp and πp collisions and their behavior as a function of the transverse momentum (p_T) has been an important test[1] of QCD.

Presently there is much experimental activity in the range of energy $\sqrt{s}\simeq 19$–24 GeV and $p_T \simeq 2$–5 GeV at CERN and Fermilab.[2–7] In this range, the variable $x_T \equiv 2p_T/\sqrt{s}$ attains fairly large values ($x_T \lesssim 0.5$), and another test of QCD becomes possible, as follows: It is known[8–10] that in QCD direct photon production is dominated by the QCD Compton and annihilation subprocesses. Suppose that one compares $\pi^- + p \to \gamma + X$ to $\pi^+ + p \to \gamma + X$; the contribution of the Compton subprocess is the same, but of the annihilation subprocess is substantially larger in the former reaction. As x_T increases, the relative importance of the annihilation subprocess increases (due to the presence of valence quarks and antiquarks in the initial state, see Sec. II). Then one predicts that, with increasing x_T (or increasing p_T at fixed s) the magnitude of $\pi^- + p \to \gamma + X$ relative to $\pi^+ + p \to \gamma + X$ substantially increases. The same holds if one compares[7] $\bar{p} + p \to \gamma + X$ to $p + p \to \gamma + X$. This prediction is an important test of QCD.

Our purpose is to study in detail direct γ production by π^- and π^+ beams at the above energy and p_T range. We consider all the important uncertainties that beset a theoretical calculation, such as the choice of the input parton (in particular gluon) distributions, of the scale parameter Λ, of the large variable Q^2, etc. We take into account all the known corrections and effects, such as higher-order [$O(\alpha_s^2)$] perturbative corrections (K factors), photon bremsstrahlung, parton-intrinsic-transverse-momentum effects, and higher-twist contributions.

Our basic conclusion is that the ratio $\sigma_\gamma^-/\sigma_\gamma^+$ of the photon production cross sections by π^-/π^+ beams is the most sensitive quantity; and it is predicted to show a clear increase with x_T. Certain preliminary data appear to contradict this prediction. Anyway, we conclude that precise measurements of $\sigma_\gamma^-/\sigma_\gamma^+$ offer another important test of QCD.

Section II presents our basic formalism; Sec. III is devoted to the input parton distributions, the corrections and the uncertainties; Sec. IV presents our results and compares them with available data; and Sec. V discusses the effect of the various corrections to the ratio $\sigma_\gamma^-/\sigma_\gamma^+$, and presents our conclusions.

II. FORMALISM

As we mentioned, the main source of the large-p_T direct photons in hadronic collisions are the QCD Compton and annihilation subprocesses (of order α_s), namely,

$$q + g \to q + \gamma \,, \tag{2.1}$$

$$q + \bar{q} \to g + \gamma \,. \tag{2.2}$$

Their differential cross sections are well known;[8–10] we give them here for completeness:

$$\frac{d\sigma^{qg}}{d\hat{t}}(\hat{s},\hat{t}) = e_q^2 \frac{1}{3}\frac{\pi\alpha\alpha_s}{\hat{s}^2}\frac{\hat{s}^2+\hat{t}^2}{-\hat{t}\hat{s}} \,, \tag{2.3}$$

$$\frac{d\sigma^{q\bar{q}}}{d\hat{t}}(\hat{s},\hat{t}) = e_q^2 \frac{8}{9}\frac{\pi\alpha\alpha_s}{\hat{s}^2}\frac{\hat{t}^2+\hat{u}^2}{\hat{t}\hat{u}} \,, \tag{2.4}$$

where $\hat{s},\hat{t},\hat{u}$ are the subprocess Mandelstam invariants ($\hat{s}+\hat{t}+\hat{u}=0$).

This work deals with the inclusive reactions

$$\pi^{\pm} + N \to \gamma + X \,, \tag{2.5}$$

where N is a nucleus and the photon is produced with center-of-mass (pseudo)rapidity η. Then denoting by $a + b \to c + \gamma$ any of the subprocesses (2.1) and (2.2) the contribution to the inclusive cross section for (2.5) is

$$E\frac{d\sigma}{d^3p}(p_T,s,\eta) = \frac{2}{\pi}\int_{x_1}^1 \frac{dx_a}{2x_a - x_T e^{\eta}} F_{a/\pi}(x_a,Q^2) \times F_{b/N}(x_b,Q^2)\frac{d\sigma^{ab}}{d\hat{t}}(\hat{s},\hat{t}) + (\eta \leftrightarrow -\eta) \,, \tag{2.6}$$

where $x_T = 2p_T/\sqrt{s}$ and

$$x_1=\frac{x_T e^{\eta}}{2-x_T e^{-\eta}},\quad x_b=\frac{x_a x_T e^{-\eta}}{2x_a-x_T e^{\eta}}\ ; \tag{2.7}$$

$F_{a/\pi}, F_{b/N}$ are parton momentum distributions in the pion and nucleus, respectively. Much of the available data correspond to integrated cross sections in the rapidity interval $\eta_1\le\eta\le\eta_2$. Thus we consider also ($\pm$ refers to $\pi^{\pm}N\to\gamma+X$):

$$\sigma_{\gamma}^{\pm}\equiv\frac{d\sigma}{dp_T}(s,p_T)=2\pi p_T\int_{\eta_1}^{\eta_2}d\eta\,E\frac{d\sigma}{d^3p}(p_T,s,\eta)\ . \tag{2.8}$$

Large-p_T photons also arise via bremsstrahlung (brems) from hard-parton-scattering subprocesses, namely,

$$a+b\to c+d+\gamma\ ; \tag{2.9}$$

there are eight distinct quark and gluon subprocesses of the type

$$a+b\to c+d\ . \tag{2.10}$$

The contribution of

$$q+q\to q+q+\gamma \tag{2.11}$$

has been calculated exactly to order α_s^2, and it was found that its dominant part arises from the kinematic configurations in which the photon is collinear with one of the final quarks. This part factorizes into the $qq\to qq$ cross section multiplied by a $q\to\gamma$ fragmentation function which is proportional to $\ln Q^2$. The remaining part ("constant piece") is very small.[11,12] A similar behavior is plausibly expected for all the brems subprocesses (2.9). Thus for all of them we calculate the dominant contribution to (2.5); this is given by the factorized form

$$\begin{aligned}E\frac{d\sigma}{d^3p}(p_T,s,\eta)&=\frac{1}{\pi}\int_{x_1}^{1}\frac{dx_a}{x_a}\int_{x_2}^{1}\frac{dx_b}{x_b}F_{a/\pi}(x_a,Q^2)F_{b/N}(x_b,Q^2)\\&\quad\times\frac{d\sigma^{ab\to cd}}{d\hat{t}}(\hat{s},\hat{t})\frac{1}{z^2}D_{\gamma/c}(z,Q^2)\\&\quad+(\eta\leftrightarrow-\eta)\ ,\end{aligned} \tag{2.12}$$

where $d\sigma^{ab\to cd}/d\hat{t}$ is the Born cross section for (2.10)[13] and

$$x_2=\frac{x_a x_T e^{-\eta}}{2x_a-x_T e^{\eta}},\quad z=\frac{x_T}{2}\left[\frac{e^{\eta}}{x_a}+\frac{e^{-\eta}}{x_b}\right]\ . \tag{2.13}$$

$D_{\gamma/c}$ is the fragmentation function of the parton c into a photon, with the form

$$D_{\gamma/c}(z,Q^2)=\frac{\alpha}{2\pi}d_{\gamma/c}(z)\ln Q^2/\Lambda^2\ . \tag{2.14}$$

For $d_{\gamma/c}(z)$ there are several available forms (see, e.g., Ref. 14); the form we use is specified in the next section. The brems contributions to the cross sections $\sigma_{\gamma}^{\pm}$ (integrated in $\eta_1\le\eta\le\eta_2$) are given by an expression similar to (2.8).

Finally, higher-twist contributions, arising, e.g., from direct interaction of the pion with a constituent of the nucleon,[9,15] may become important near the edge of the phase space, i.e., near $x_T=1$ and $\theta_{\text{c.m.}}<90°$; this may particularly hold for the integrated cross section (2.8) of $\pi^-N\to\gamma+X$. We shall use the formalism of Ref. 15.

III. PARTON DISTRIBUTIONS, CORRECTIONS, AND UNCERTAINTIES

We use quark and gluon distributions in the pion recently determined in Ref. 16 by simultaneous fitting dimuon and J/ψ production data in πN processes. For consistency, we also use the parton distributions in the nucleon given in Ref. 17, which are input in the determination of the above pion distribution functions. All these distributions include scale violations calculated in the leading-logarithm QCD approximation.

In view of the uncertainties, mainly regarding the gluon distribution, we consider both distribution sets 1 and 2 given in Refs. 16 and 17. These differ in the choice of $F_{g/p}$, the gluon distribution in the proton, and in the resulting fitted value of the QCD scale parameter Λ. Specifically, at $Q^2=Q_0^2=4$ GeV^2 we have

Set 1 ($\Lambda=0.2$ GeV):

$$F_{g/p}(x,Q_0^2)=1.56(1+9x)(1-x)^6\ , \tag{3.1a}$$

$$F_{g/\pi}(z,Q_0^2)=0.888(1+6x)(1-x)^{3.11}\ . \tag{3.1b}$$

Set 2 ($\Lambda=0.4$ GeV):

$$F_{g/p}(x,Q_0^2)=0.879(1+9x)(1-x)^4\ , \tag{3.2a}$$

$$F_{g/\pi}(x,Q_0^2)=0.794(1+6x)(1-x)^{2.89}\ . \tag{3.2b}$$

Clearly, set 2 contains somewhat broader gluon distributions. As in Refs. 16 and 17, we assume SU(3) symmetric sea, namely, $F_{\bar{u}/p}=F_{\bar{d}/p}=F_{s/p}$ and $F_{\bar{u}/\pi^+}=F_{\bar{d}/\pi^+}=F_{s/\pi^+}$.

Regarding the function $d_{\gamma/c}(z)$ of the photon brems contribution [Eq. (2.14)] we use the parametrization[18]

$$d_{\gamma/c}(z)=2z^{-0.6}\sum_{n=0}^{4}a_n^c z^n\ . \tag{3.3}$$

The coefficients a_n^c are given in Ref. 18 [see also Eqs. (2.16)–(2.18) of Ref. 14]. This parametrization provides an adequate representation of the exact result[18] even for large z; and in Ref. 14 it was found to give intermediate results among various proposed forms of $d_{\gamma/c}(z)$.

Note that in the leading-logarithm approximation a gluon can also fragment into a photon as a result of the intermediate transition $g\to q\bar{q}$. However, such contributions are very small. In fact, at $\sqrt{s}=23.75$ GeV and $p_T=2$ GeV we find that 87% of the total brems contribution is due to the subprocesses

$$q+q\to q+(q\to q\gamma)\ , \tag{3.4}$$

$$g+q\to g+(q\to q\gamma)\ ; \tag{3.5}$$

at $p_T=5$ GeV, (3.4) and (3.5) account for 98% of the brems contribution. Similar results were found in Ref. 14. Thus, when presenting our results in Sec. IV, we display explicitly only the contributions of (3.4) and (3.5);

nevertheless the total brems contribution we present comprises all possible collinear photon emission configurations.

The choice of the scale parameter Λ in the QCD running coupling strength

$$\alpha_s(Q^2)=\frac{12\pi}{33-2f}\frac{1}{\ln(Q^2/\Lambda^2)} \tag{3.6}$$

(f=number of flavors), and in Eq. (2.14), is an additional uncertainty. The data analysis of the CERN-Dortmund-Heidelberg-Saclay (CDHS) collaboration gives[19] $\Lambda=0.2$ GeV. Doubling this, at $p_T\simeq 4$ GeV results in Born contributions larger by a factor of ~ 1.5.

Yet another uncertainty arises from the choice of the scale ("large variable") Q^2. Our results correspond to $Q^2=p_T{}^2$. This choice gives almost similar results with $Q^2=-\hat{t}/2$. The choice $Q^2=2p_T{}^2$ (similar to $Q^2=-\hat{t}$) is found to lead to cross sections smaller by a factor $\lesssim 1.5$.

The experiments we consider correspond to not too large $\sqrt{s}$ and p_T. Then, as functions of p_T, the photon inclusive cross sections are relatively steep and the effect of parton-intrinsic-transverse-momentum k_T is important. Comparisons of QCD calculations with CERN ISR data for $p+p\to\gamma+X$ show that a relatively large $\langle k_T\rangle$ is required to account for the experimental cross sections at $p_T\sim 4$ GeV (Refs. 20 and 14). We take into account this effect assuming that the initial partons are on shell and using a Gaussian k_T distribution with

$$\langle k_T\rangle=0.7\text{ GeV} . \tag{3.7}$$

It will be seen that for $p_T\lesssim 5$ GeV the k_T effect is quite significant.

Now we consider higher-order [$O(\alpha_s{}^2)$] perturbative corrections (K factors), which arise from loop graphs involving gluons and from gluon brems. For the subprocesses (2.1) and (2.2) complete calculations have been carried in Ref. 21. In view of the very large number of terms involved explicit forms are not available. However, for the energies of interest here, in the range $2\lesssim p_T\lesssim 6$ GeV and for $|\eta|$ not too large the resulting K factors (corresponding to the scale $Q^2=p_T{}^2$) can be approximated by the forms[22]

$$K(qg\to\gamma q)\simeq 2.3,\quad K(q\bar{q}\to\gamma g)=\sum_{n=0}^{3}a_n p_T{}^n , \tag{3.8}$$

where

$$\begin{aligned} &a_0=4.256,\quad a_1=-1.191 ,\\ &a_2=0.174,\quad a_3=-8.7\times 10^{-3} . \end{aligned} \tag{3.9}$$

We use the forms (3.8) in the subsequent calculations. With these forms, at the higher p_T ($\simeq 6$ GeV), $K(qg\to\gamma q)$ somewhat exceeds $K(q\bar{q}\to\gamma g)$; at the lower p_T ($\simeq 2.5$ GeV), $K(qg\to\gamma q)\simeq K(q\bar{q}\to\gamma g)$.

Approximate K factors determined from loop graphs in the soft-gluon limit and from certain collinear gluon brems configurations, have the form

$$K=1+\frac{\alpha_s(Q^2)}{2\pi}C\pi^2 , \tag{3.10}$$

where C is a combination of color factors. With the definition of corrections (factorization prescription) of Ref. 23 one finds corresponding to the subprocesses (2.1) and (2.2) (Ref. 24)

$$C(qg\to\gamma q)=\frac{N}{2}+\frac{C_F}{3},\quad C(q\bar{q}\to\gamma g)=C_F , \tag{3.11}$$

where $N=3$ and $C_F=\frac{4}{3}$ in color SU(3).[25] The corrections corresponding to (3.10) and (3.11) are somewhat smaller than those of (3.8) and (3.9); however, as we will discuss (end of Sec. IV), the difference is within the various uncertainties that beset the calculations.

For the subprocesses (2.10), which are involved in the photon brems contributions, complete K factors are not available, apart from the simplest case $qq'\to qq'$ (nonidentical quark scattering). Data on large-p_T jet production at the CERN collider[26] support an enhancement factor $K\sim 2$. Approximate K factors of the form[27] (3.10) lead to a similar result. In view of the relative smallness ($\sim 20\%$) of the photon brems contribution and to keep our calculation as clean as possible, we simply take for all the subprocesses (2.10)

$$K(ab\to cd)=2 . \tag{3.12}$$

IV. RESULTS

We present our results for the energies and rapidities of the various experiments (with pion beams) in progress. We use the parton distributions of set 2 [Eqs. (3.2)], but we make certain comparisons using also set 1.

NA3 collaboration ($\sqrt{s}=19.4$ GeV)

This collaboration uses an isoscalar carbon target and has already presented[2] preliminary data for cross sections

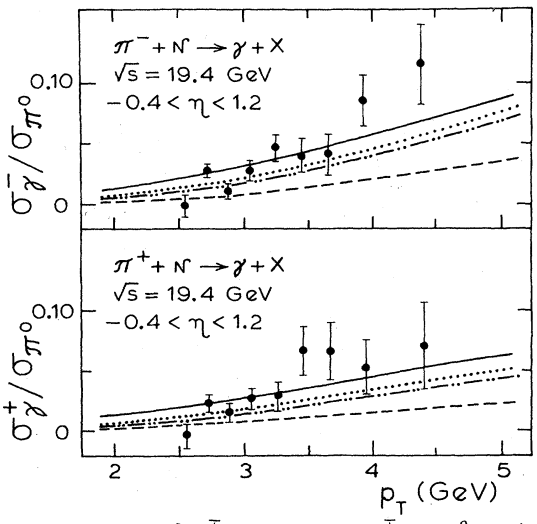

FIG. 1. Ratios of $\pi^{\mp}N\to\gamma+X$ to $\pi^{\mp}N\to\pi^0+X$ inclusive cross sections integrated in the rapidity interval $-0.4<\eta<1.2$. Dashed curves, Born contributions [subprocesses (2.1) and (2.2)]. Dash—double-dotted curve, with $O(\alpha_s{}^2)$ corrections [K factors (3.8), (3.9)]. Dotted curve, with photon brems contributions. Solid curve with parton-intrinsic k_T. Data from Ref. 2 (NA3 collaboration).

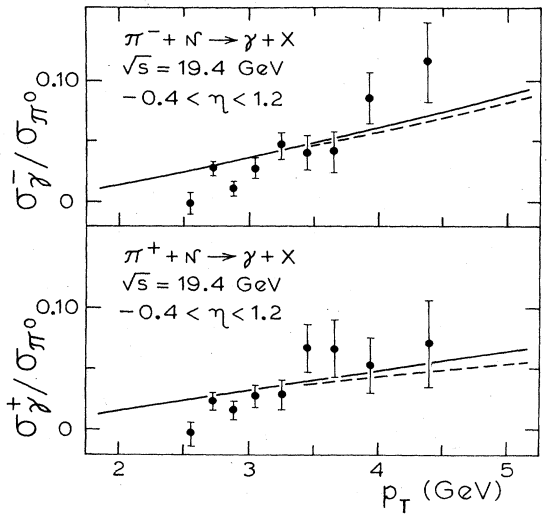

FIG. 2. Ratios as in Fig. 1 calculated with parton distributions of set 1 (dashed curves) and of set 2 (solid curve). In addition to the Born contributions, $O(\alpha_s^2)$ corrections, photon brems, and k_T effects are included.

$\sigma_\gamma^\mp$ [Eq. (2.8)] integrated in the c.m. rapidity range $-0.4 < \eta < 1.2$. The data are given (Fig. 1) in the form of ratios $\sigma_\gamma^\mp / \sigma_{\pi^0}$, where σ_{π^0} denote cross sections for $\pi^\mp N \to \pi^0 + X$ integrated in the same rapidity range.

Figure 1 compares these data with our results. As in Ref. 2, to determine σ_{π^0} we use the parametrization of Donaldson *et al.*[28] for $\pi^\mp p \to \pi^0 + X$; and to account for nuclear effects we multiply by a factor A^α, $\alpha = 1.12$ (Ref. 2). The most important effects are clearly displayed: The Born contributions [dashed curves; subprocesses (1.1) and (1.2)], are significantly enhanced by the inclusion of $O(\alpha_s^2)$ QCD corrections [dash-double-dotted curves; Eqs. (3.8) and (3.9)]; photon brems (dotted curves) further enhances, to some extent, the results; finally, the effect of parton-intrinsic k_T (solid curves) is quite significant through most of the p_T range of the data.

Figure 2 presents a comparison of results for set 1 (dashed curves) versus set 2 (solid curves), for the same ratios $\sigma_\gamma^\mp / \sigma_{\pi^0}$. In each case the same effects as in Fig. 1 are included. Clearly the difference is not significant; these data are well accounted for by either set. We proceed by using mostly set 2.

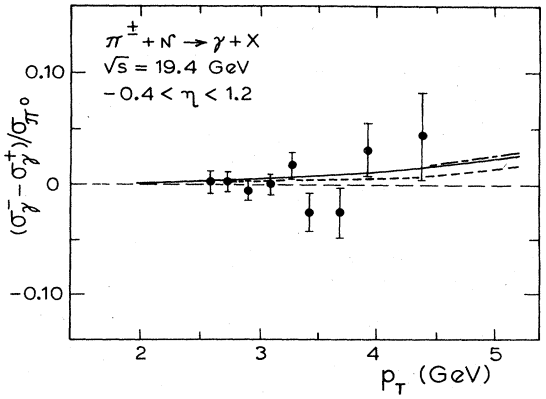

FIG. 3. Inclusive-cross-section difference for $\pi^- N \to \gamma + X$ and $\pi^+ N \to \gamma + X$ integrated in $-0.4 < \eta < 1.2$, normalized to the corresponding π^0 cross sections. Dashed and solid curves as in Fig. 1. Long-dash—short-dashed curve, including higher-twist effects. Data from Ref. 2.

The same collaboration[2] has also presented preliminary data for the difference $(\sigma_\gamma^- / \sigma_{\pi^0}) - (\sigma_\gamma^+ / \sigma_{\pi^0})$ (Fig. 3). In view of the fact that the photon brems contributions are almost the same for σ_γ^- and σ_γ^+ (see below), the difference $\sigma_\gamma^- - \sigma_\gamma^+$ is a good measure of the importance of the $q\bar{q} \to \gamma g$ subprocess. Figure 3 presents our Born term (dashed curve) plus the contribution of $O(\alpha_s^2)$ corrections, photon brems, and parton's k_T (solid curve). It also presents the addition of a higher-twist contribution (long-dash—short-dashed curve);[15] clearly, the effect is very small and is neglected in subsequent comparisons with data. Unfortunately, apart from limited statistics, by dividing $\sigma_\gamma^\mp$ by σ_{π^0}, much of the sensitivity of the results is lost; the data are consistent with all our results.

In Fig. 4 we present our results for the ratio $\sigma_\gamma^- / \sigma_\gamma^+$ (curves as in Fig. 1). The ratio of the Born term contributions decreases more and more as we add $O(\alpha_s^2)$ corrections, photon brems, and partons' k_T; nevertheless, in all cases $\sigma_\gamma^- / \sigma_\gamma^+$ shows a clear increase with p_T (see also below). Evidently, $\sigma_\gamma^- / \sigma_\gamma^+$ provides the most sensitive quantity for a QCD test.

Figures 5 and 6 display some of the individual contributions to the integrated cross sections $d\sigma/dp_T$ [Eq. (2.8)] of $\pi^- N \to \gamma + X$ and $\pi^+ N \to \gamma X$. They also give [denoted

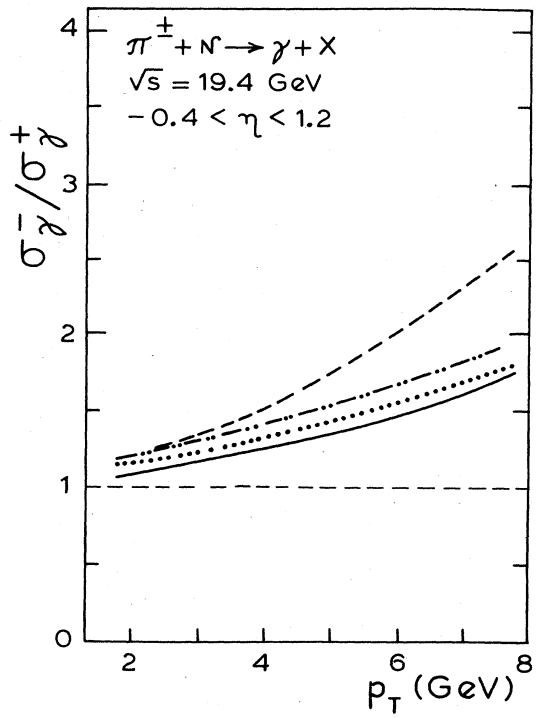

FIG. 4. Ratio of inclusive cross sections $\pi^- N \to \gamma + X$ and $\pi^+ N \to \gamma + X$ integrated in $-0.4 < \eta < 1.2$. Notation as in Fig. 1.

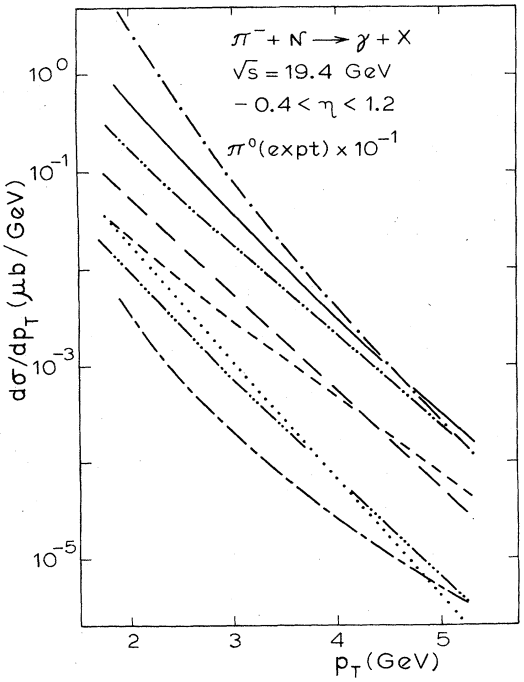

FIG. 5. Contributions to the inclusive $\pi^- N \rightarrow \gamma + X$ cross section integrated in $-0.4 < \eta < 1.2$. Long-dashed curve, Born contribution of $qg \rightarrow \gamma q$. Short-dashed curve, Born contribution of $q\bar{q} \rightarrow \gamma g$. Dash—two-dotted curve, sum of Born together with $O(\alpha_s^2)$ corrections (3.8). Solid curve, total contribution (including all photon brems contributions and partons' k_T). Dash—three-dotted curve, Born brems contribution from $qq \rightarrow qq\gamma$. Dotted curve, Born brems contribution from $qg \rightarrow gq\gamma$. Long-dash—short-dashed curve, higher-twist contribution. π^0(expt) denotes the corresponding $\pi^- p \rightarrow \pi^0 + X$ cross section from Ref. 28.

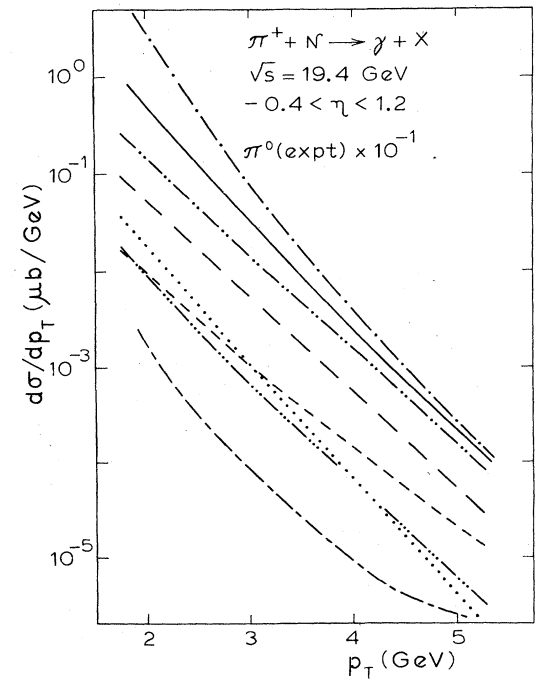

FIG. 6. As in Fig. 5 for $\pi^+ N \rightarrow \gamma + X$.

by π^0(expt)] the corresponding cross sections for $\pi^{\mp} p \rightarrow \pi^0 + X$ used in our determination of $\sigma_\gamma^{\mp}/\sigma_{\pi^0}$ (not multiplied by A^α). Notice that the main photon brems contributions [$qq \rightarrow q + (q \rightarrow q\gamma)$, dash—triple-dotted curve, and $gq \rightarrow g + (q \rightarrow q\gamma)$, dotted curve] are almost the same for $\pi^- N \rightarrow \gamma + X$ and $\pi^+ N \rightarrow \gamma + X$. The same figures also display the higher-twist contributions (long-dash—short-dashed curves); these are very small, and only for $\pi^- N \rightarrow \gamma + X$ and at the highest p_T become comparable to photon brems. Notice that our higher-twist contributions (Figs. 5 and 6) are somewhat smaller and drop with p_T faster than those estimated in Ref. 15. The reason is that we use a running $\alpha_s(Q^2)$ [Eq. (3.6)] and parton distributions including scale violations whereas Ref. 15 uses a fixed $\alpha_s = 0.3$ and scaling parton distributions.

NA24 collaboration ($\sqrt{s} = 23.75$ GeV)

This collaboration uses a hydrogen target and has presented[3] preliminary data for cross sections integrated in the c.m. rapidity $-0.7 < \eta < 0.9$.

Figure 7 presents our results and compares them with the data for $\sigma_\gamma^{\mp}/\sigma_{\pi^0}$, and Fig. 8 for $\sigma_\gamma^-/\sigma_\gamma^+$. σ_{π^0} denote cross sections for $\pi^{\mp} p \rightarrow \pi^0 + X$ integrated in the above rapidity range. Our σ_{π^0} are determined from data of the same collaboration,[3] and are shown on Figs. 9 and 10 [denoted by π^0(expt)]; they correspond to[3] $d\sigma(\pi^- p \rightarrow \pi^0 X)/dp_T = d\sigma(\pi^+ p \rightarrow \pi^0 X)/dp_T$.

Figure 7 displays the hierarchy of our most important contributions to $\sigma_\gamma^{\mp}/\sigma_{\pi^0}$ (curves as in Fig. 1). On the

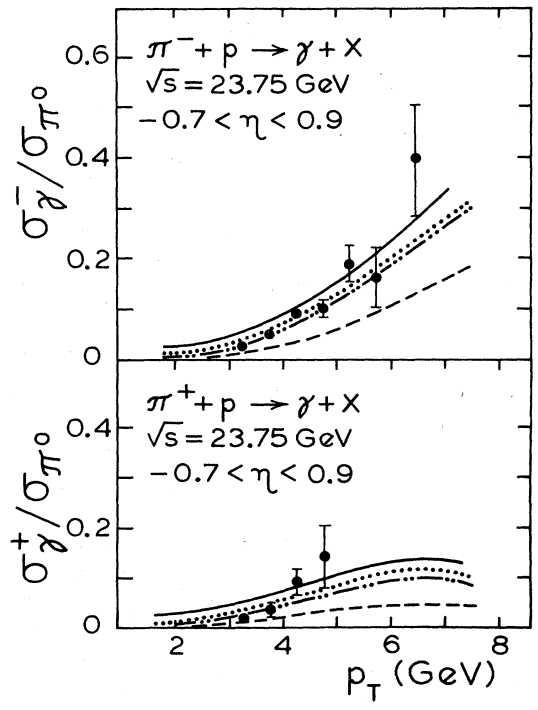

FIG. 7. Ratios of $\pi^{\mp} p \rightarrow \gamma + X$ to $\pi^{\mp} p \rightarrow \pi^0 + X$ inclusive cross sections integrated in $-0.7 < \eta < 0.9$. Notation as in Fig. 1. Data from Ref. 3 (NA24 collaboration).

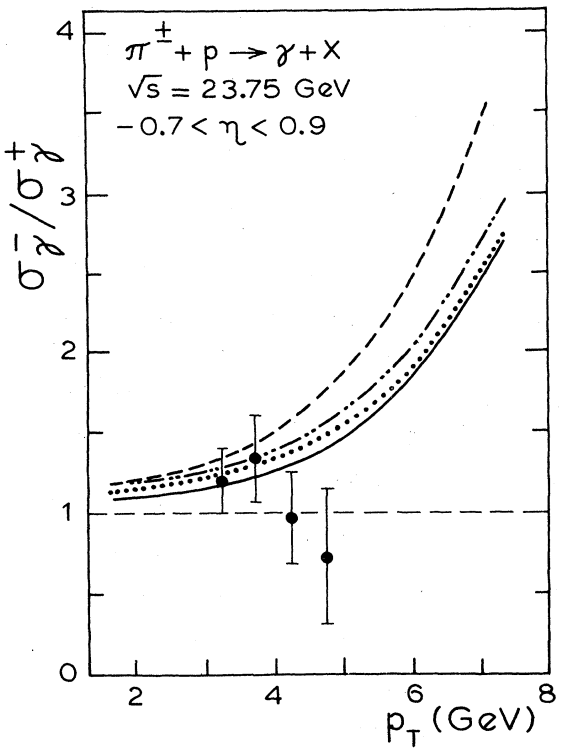

FIG. 8. Ratio of the inclusive cross sections $\pi^- p \rightarrow \gamma + X$ and $\pi^+ \rightarrow \gamma + X$ integrated in $-0.7 < \eta < 0.9$. Notation as in Fig. 1. Preliminary data from Ref. 3.

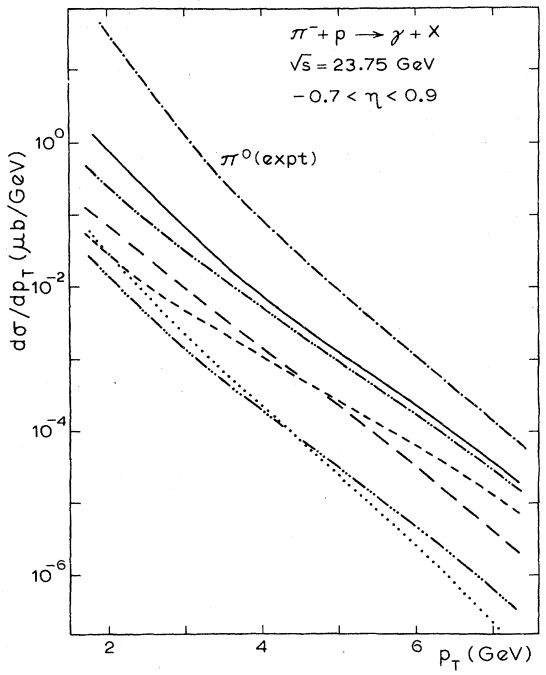

FIG. 9. Contributions to the inclusive $\pi^- p \rightarrow \gamma + X$ cross section integrated in $-0.7 < \eta < 0.9$. Notation as in Fig. 5. π^0(expt) denotes the corresponding $\pi^- p \rightarrow \pi^0 + X$ cross section determined from data of Ref. 3.

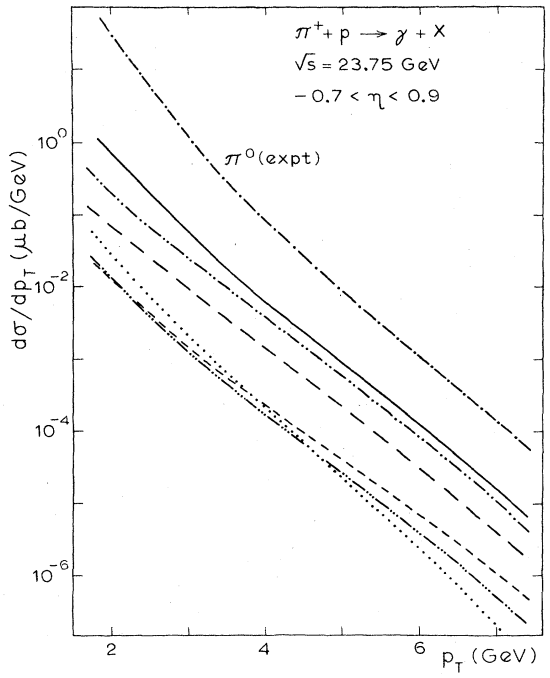

FIG. 10. As in Fig. 9 for $\pi^+ p \rightarrow \gamma + X$.

whole our final results (solid curves) are in fair agreement with the data, in particular at the highest p_T.

More interesting is the behavior of the ratio $\sigma^-_\gamma / \sigma^+_\gamma$ as a function of p_T (Fig. 8). As in Fig. 4, inclusion of the various effects tends to decrease this ratio; however, there remains a clear increase with p_T which is not supported by the preliminary data. We return below to this point.

Some of the individual contributions to the integrated cross sections $d\sigma/dp_T$ of $\pi^{\mp} p \rightarrow \gamma + X$ are shown in Figs. 9 and 10.

E-706 collaboration ($\sqrt{s} = 19.4$ GeV)

This collaboration has produced data[5,6] on $\pi^+ + N \rightarrow \gamma + X$ with N=C, Al, and Be targets, at $\theta_{\text{c.m.}} = 90°$ ($\eta = 0$). Most of the data are for carbon, and we present results for both $\pi^{\mp} N \rightarrow \gamma + X$ for N=C.

Figure 11 presents our results for $\pi^+ N \rightarrow \gamma + X$ together with the data.[5,6] The solid curve [including Born, $O(\alpha_s{}^2)$ corrections, photon brems, and parton-k_T effect] corresponds to set 2; the dashed—four-dotted curve (including the same) to set 1. Both results are in agreement with the data.

Figure 12 presents our results for $\pi^- N \rightarrow \gamma + X$. Again, the difference between sets 1 and 2 is small. In both Figs. 11 and 12 the long-dash—short-dashed curves show the higher-twist contributions; they are small even for $\pi^- N \rightarrow \gamma + X$.

Figure 13 shows our results for the ratios of $E\, d\sigma(\pi^{\mp} N \rightarrow \gamma X)/d^3p$ divided by $E\, d\sigma(\pi^{\mp} N \rightarrow \pi^0 X)/d^3p$. The latter have been determined from a best fit to data for $\pi^+ N \rightarrow \pi^0 + X$ of the same experiment,[6,29] and are shown in Figs. 11 and 12 [denoted π^0(expt)]; we have as-

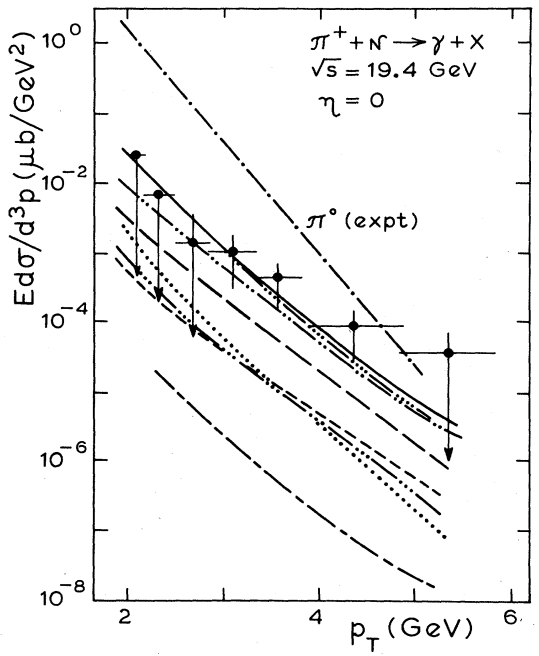

FIG. 11. Contributions to the inclusive $\pi^+N \to \gamma + X$ cross section at $\theta_{c.m.} = 90°$ ($\eta = 0$). Notation as in Fig. 5 (calculated with parton distributions of set 2). Dash—four-dotted curve, total contribution calculated with set 1. Data from Refs. 5 and 6 (E-706 collaboration). π^0(expt) is a best fit to data of the same references.

sumed $E\,d\sigma(\pi^- N \to \pi^0 X)/d^3p = E\,d\sigma(\pi^+ N \to \pi^0 X)/d^3p$.

Finally, Fig. 14 shows our results for the ratio of $E\,d\sigma(\pi^- N \to \gamma X)/d^3p$ and $E\,d\sigma(\pi^+ N \to \gamma X)/d^3p$; as in Figs. 11 and 12, the solid curve is our final result with set

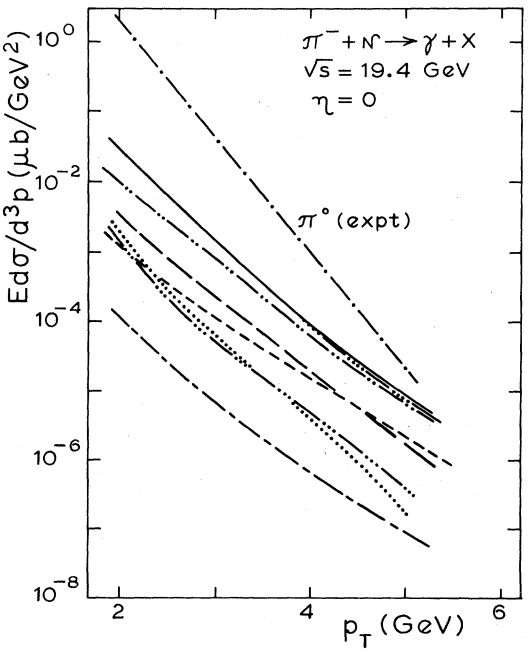

FIG. 12. As in Fig. 11 for $\pi^- N \to \gamma + X$.

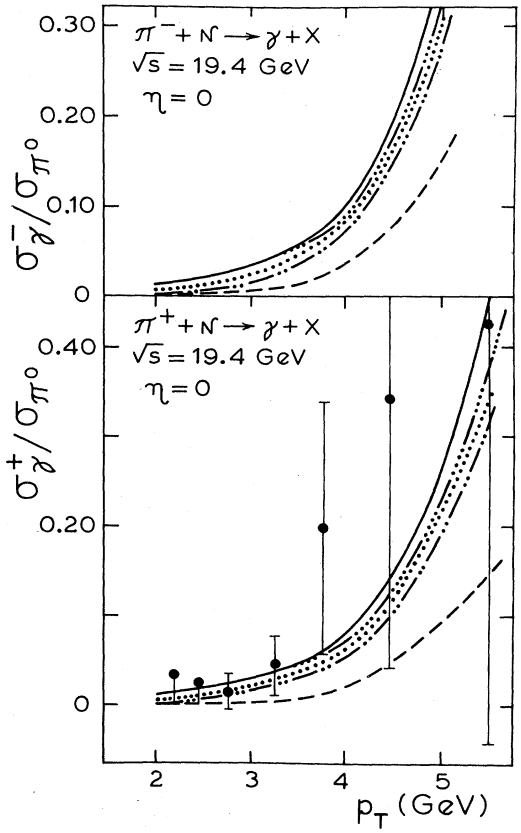

FIG. 13. Ratios of $\pi^\mp N \to \gamma + X$ to $\pi^\mp N \to \pi^0 + X$ inclusive cross sections at $\theta_{c.m.} = 90°$ ($\eta = 0$). Notation as in Fig. 1 (calculated with parton distributions of set 2). Dash—four-dotted curves, total contribution calculated with set 1. Data from Refs. 5 and 6.

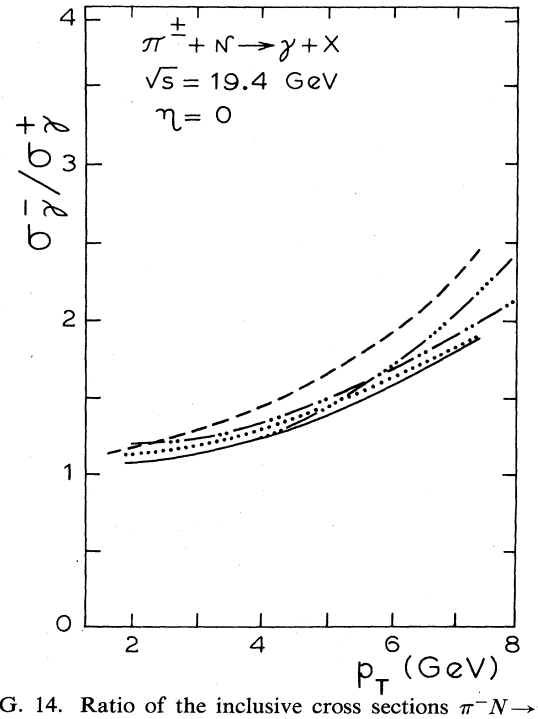

FIG. 14. Ratio of the inclusive cross sections $\pi^- N \to \gamma + X$ and $\pi^+ N \to \gamma + X$ at $\theta_{c.m.} = 90°$. Notation as in Fig. 13.

2, the dash—four-dotted curve with set 1. With either set, there is clear increase of the ratio with p_T.

WA70 collaboration ($\sqrt{s}=22.9$ GeV)

This uses a hydrogen target and anticipates results for several values of the Feynman variables x_F in the range[4,30] $-0.4 \leq x_F \leq 0.4$. We present results for $\pi^{\mp}p \to \gamma + X$ cross sections at $x_F=0$ as well as integrated in the above range.

Figures 15 and 16 show some of our individual contributions at $x_F=0$ and Figs. 17 and 18 for $-0.4 \leq x_F \leq 0.4$. Again, our final $\pi^{\mp}p \to \gamma + X$ cross sections calculated with set 2 (solid curves) or set 1 (dash—four-dotted curves) differ little; and the higher-twist contributions (long-dash—short-dashed curves) are very small, apart from $\pi^- p \to \gamma + X$, $-0.4 \leq x_F \leq 0.4$ (Fig. 17) at the highest p_T.

Figure 19 shows the ratios of $E\,d\sigma(\pi^{\mp}p \to \gamma X)/d^3p$ divided by $E\,d\sigma(\pi^{\mp}p \to \pi^0 X)/d^3p$ at $x_F=0$. For the latter we have used the parametrization of Donaldson *et al.*;[28] anyway, they are shown in Figs. 15 and 16 [denoted π^0(expt)]. Figure 20 shows the ratios $\sigma_\gamma^{\mp}/\sigma_{\pi^0}$ for cross sections integrated in the range $-0.4 \leq x_F \leq 0.4$. In both Figs. 19 and 20 the hierarchy of the most important contributions is displayed.

Finally, Fig. 21 shows our results for the ratio $\sigma_\gamma^-/\sigma_\gamma^+$ (integrated cross sections) and for the ratio $E\,d\sigma(\pi^- p \to \gamma X)/d^3p \,/\, E\,d\sigma(\pi^+ p \to \gamma X)/d^3p$ at $x_F=0$. As in Figs. 4, 8, and 14, there is a clear increase of these ratios with p_T.

We conclude this section with a comparison of the ratio $\sigma_\gamma^-/\sigma_\gamma^+$ at $\sqrt{s}=23.75$ GeV (Fig. 22) calculated with the K factors of Eqs. (3.8) (vertical-dash band and dots) and with the approximate K factors of Eqs. (3.10) and (3.11) (horizontal-dash band and dashed curve). In each case the upper boundary corresponds to set 1, the lower to set 2. The difference is not very significant, in particular in view of the additional uncertainties [choice of Λ, Q^2, $\langle k_T \rangle$, fragmentation function $d_{\gamma/c}(z)$, etc.] discussed in Sec. III.

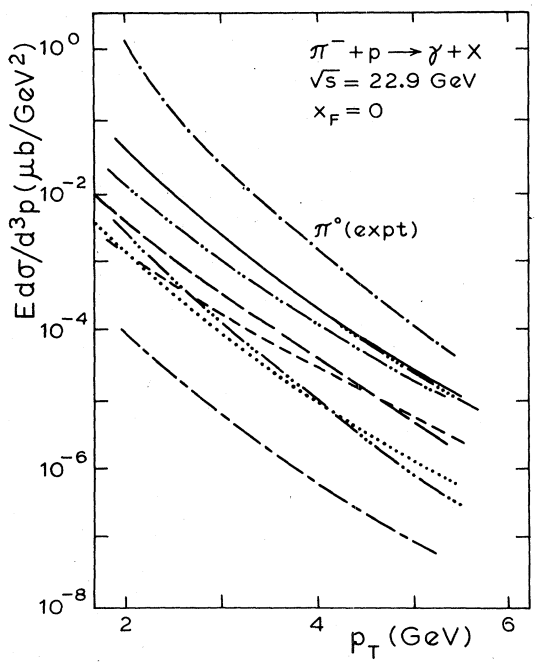

FIG. 15. Contributions to the inclusive $\pi^- p \to \gamma + X$ cross sections at $\theta_{c.m.}=90°$ ($x_F=0$). Notation as in Figs. 1 and 11. π^0(expt) denotes the corresponding $\pi^- p \to \pi^0 + X$ cross section of the parametrization of Donaldson *et al.* (Ref. 28).

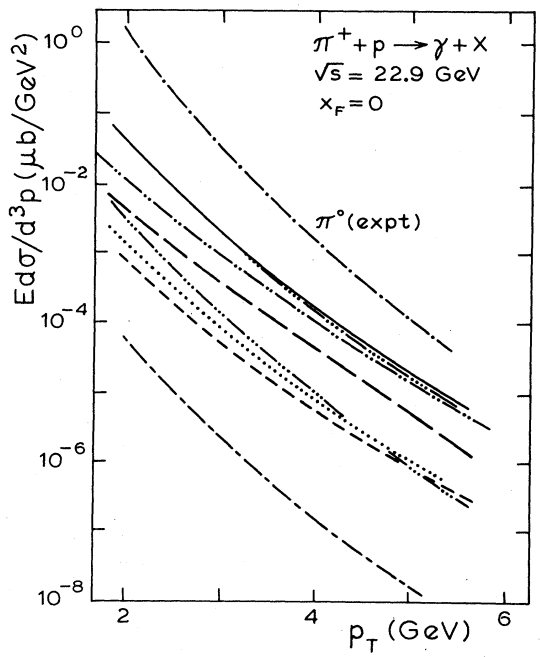

FIG. 16. As in Fig. 15 for $\pi^+ p \to \gamma + X$.

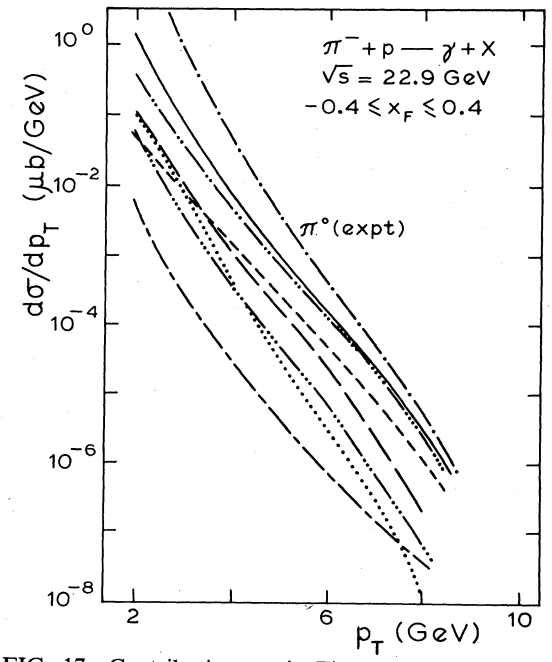

FIG. 17. Contributions as in Fig. 15 ($\pi^- p \to \gamma + X$) but integrated in the range $-0.4 \leq x_F \leq 0.4$.

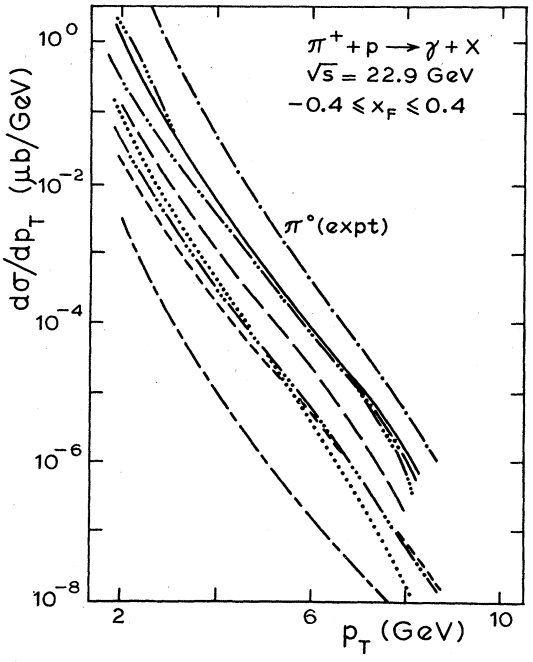

FIG. 18. As in Fig. 17 for $\pi^+ p \rightarrow \gamma + X$.

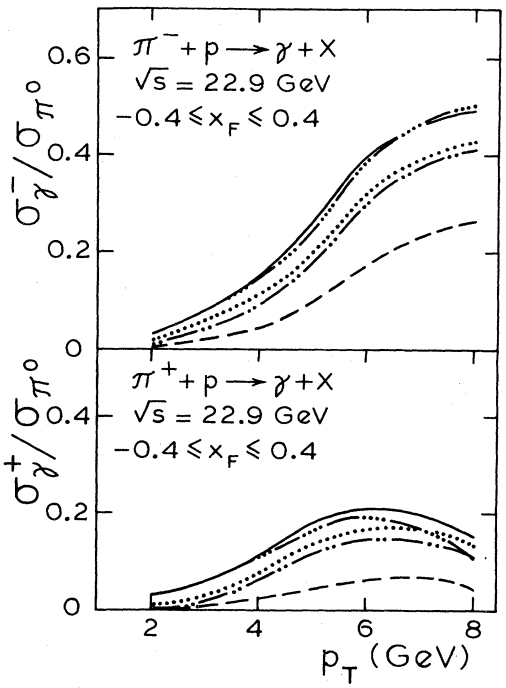

FIG. 20. As in Fig. 19 but integrated in $-0.4 \leq x_F \leq 0.4$.

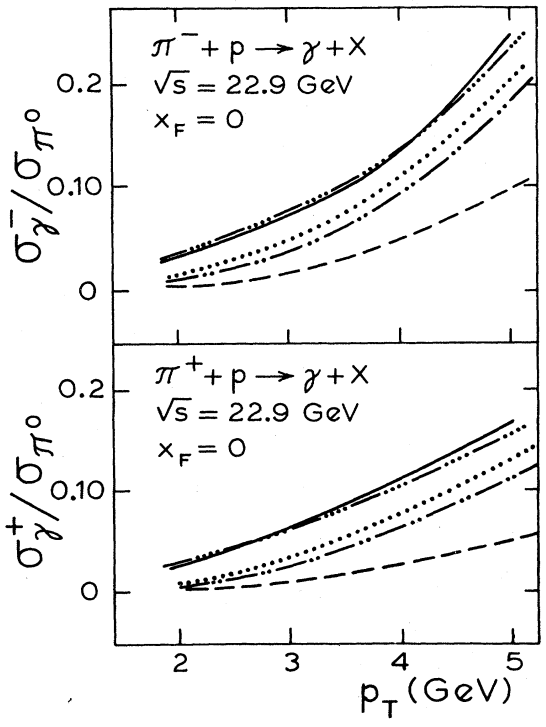

FIG. 19. Ratios of $\pi^{\mp} p \rightarrow \gamma + X$ to $\pi^{\mp} p \rightarrow \pi^0 + X$ inclusive cross sections at $\theta_{\text{c.m.}} = 90°$ ($x_F = 0$). Notation as in Figs. 1 and 13.

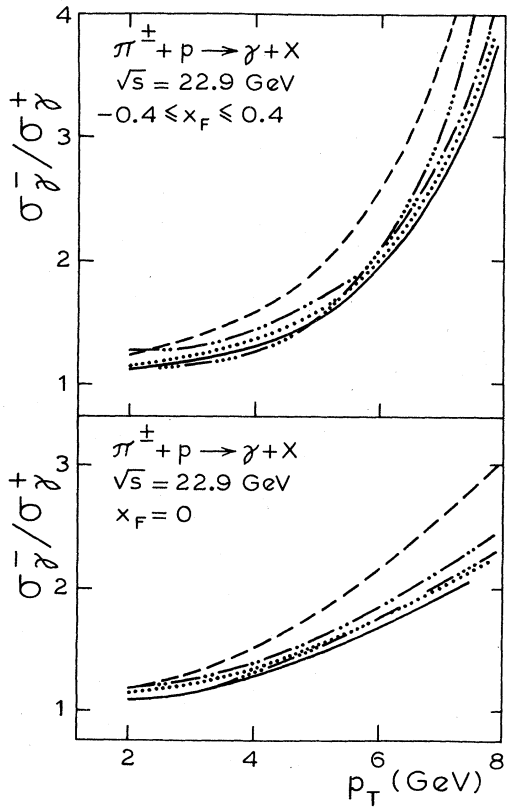

FIG. 21. Ratios of inclusive cross sections $\pi^- p \rightarrow \gamma + X$ and $\pi^+ p \rightarrow \gamma + X$ at $x_F = 0$ and integrated in $-0.4 \leq x_F \leq 0.4$. Notation as in Figs. 1 and 13.

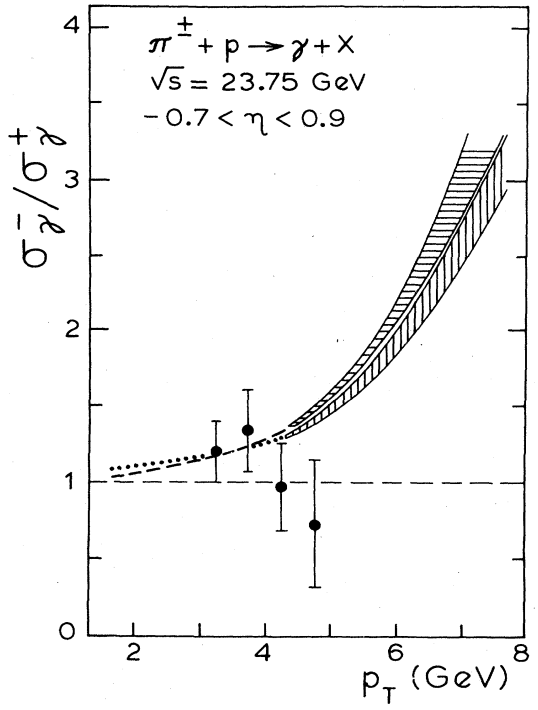

FIG. 22. Ratio of the inclusive cross sections $\pi^- p \rightarrow \gamma + X$ and $\pi^+ p \rightarrow \gamma + X$ integrated in $-0.7 \leq \eta \leq 0.9$. Vertical-dash band and dotted curve, K factors of (3.8). Horizontal-dash band and dashed curve, approximate K factors of (3.10) and (3.11). The upper (lower) boundary of each band corresponds to parton distributions of set 1(2). Preliminary data from Ref. 3.

V. THE RATIO $\sigma_\gamma^- / \sigma_\gamma^+$ AND CONCLUSIONS

Clearly the ratio $\sigma_\gamma^- / \sigma_\gamma^+$ is the most sensitive quantity for a test of the QCD prediction regarding the increase with p_T of the relative importance of the annihilation process (2.2). The change of this ratio due to the most important effects (Figs. 4, 8, and 14), can be qualitatively understood as follows.

First, notice that any effect that enhances the contribution of $qg \rightarrow \gamma q$ relative to $q\bar{q} \rightarrow \gamma g$ tends to significantly decrease $\sigma_\gamma^- / \sigma_\gamma^+$. Also, any effect that adds to $\pi^- N \rightarrow \gamma X$ and $\pi^+ N \rightarrow \gamma X$ an equal amount tends to decrease $\sigma_\gamma^- / \sigma_\gamma^+$ but to a lesser extent.

Regarding the effect of the $O(\alpha_s^2)$ corrections, we noted in Sec. III [after Eq. (3.9)] that at large p_T (~ 6 GeV) Eqs. (3.8) imply $K(qg \rightarrow \gamma q) > K(q\bar{q} \rightarrow \gamma g)$. Hence at large p_T the $O(\alpha_s^2)$ corrections tend to significantly decrease $\sigma_\gamma^- / \sigma_\gamma^+$ relative to its Born value (dash—double-dotted versus dashed curves in Figs. 4, 8, and 14). At lower p_T (2—3 GeV) Eqs. (3.8) give $K(qg \rightarrow \gamma q) \simeq K(q\bar{q} \rightarrow \gamma g)$; then $\sigma_\gamma^- / \sigma_\gamma^+$ decreases but to a lesser extent.

Regarding photon brems, it has been found (Sec. IV) that it gives about equal (and not too large) contributions in $\pi^- N \rightarrow \gamma + X$ and $\pi^+ N \rightarrow \gamma + X$. Then $\sigma_\gamma^- / \sigma_\gamma^+$ further decreases, but not much (dotted lines).

Finally regarding the parton-k_T effect, it is slightly bigger in $\pi^- N \rightarrow \gamma X$, because as functions of p_T the cross sections are somewhat steeper than those of $\pi^+ N \rightarrow \gamma X$ (due to a smaller amount of the relatively flat $q\bar{q} \rightarrow \gamma g$ contribution). Thus $\sigma_\gamma^- / \sigma_\gamma^+$ further decreases (solid curves), in particular at the lower p_T where the k_T effect is large.

Now the important point is that, with all these effects taken into account, the ratio $\sigma_\gamma^- / \sigma_\gamma^+$ is still predicted to show a clear increase with p_T. Moreover, as we discussed, the uncertainties in the calculation do not change this prediction, and the difference with the preliminary data of Ref. 3 (Figs. 8 and 22) is not accounted for.

We may conclude that precise measurements of $\sigma_\gamma^- / \sigma_\gamma^+$ will constitute another important test of QCD. In view of the present experimental activity[2–7] we expect that such measurements will be available in the near future.

ACKNOWLEDGMENTS

We would like to thank Dr. K. Pretzl for discussions and a private communication, and Dr. S. Conetti, Dr. Y. Karyotakis, and Dr. D. Ryan for discussions. This work was supported in part by the Natural Sciences and Engineering Research Council of Canada and by the Quebec Department of Education.

*On leave of absence from Department of Physics, National Technical University, Athens, Greece.

[1] T. Ferbel and W. Molzon, Rev. Mod. Phys. **56**, 181 (1984).

[2] J. Badier *et al.* (NA3 collaboration), Report No. CERN-EP/84-101 (unpublished); in *Proceedings of the XXII International Conference on High Energy Physics, Leipzig, 1984,* edited by A. Meyer and E. Wieczorek (Academie der Wissenschaften der DDR, Zeuthen, DDR, 1984).

[3] C. De Marzo *et al.* (NA24 collaboration), in *Proceedings of the 7th Warsaw Symposium on Elementary Particle Physics, Kazimierz, Poland, 1984,* edited by Z. Ajduk (Institute of Theoretical Physics, Warsaw University, Warsaw, 1984); K. Pretzl, in *Proceedings of the XXII International Conference on High Energy Physics, Leipzig, 1984* (Ref. 2).

[4] M. Martin *et al.* (WA70 CERN—University of Geneva collaboration) (unpublished).

[5] M. McLaughlin *et al.* (E-706 Fermilab-Michigan-Minnesota-Northeastern-Rochester collaboration), Phys. Rev. Lett. **51**, 971 (1983).

[6] J. Povlis, Ph.D. thesis, University of Minnesota, Minneapolis, 1984.

[7] B. Cox *et al.* (E-705 Arizona-Athens-Duke-Fermilab-McGill-Northwestern-Shandong collaboration) (unpublished).

[8] F. Halzen and D. Scott, Phys. Rev. D **18**, 3378 (1978).

[9] R. Ruckl, S. Brodsky, and F. Gunion, Phys. Rev. D **18**, 2469 (1978).

[10] A. P. Contogouris, S. Papadopoulos, and M. Hongoh, Phys. Rev. D **19**, 2607 (1979).

[11]P. Aurenche and J. Lindfors, Nucl. Phys. **B168**, 296 (1980).
[12]A. P. Contogouris, S. Papadopoulos, and C. Papavassiliou, Nucl. Phys. **B179**, 461 (1981); J. Kripfganz *et al.*, in *Proceedings of the XVth Rencontre de Moriond,* edited by J. Tran Thanh Van (Editions Frontières, Dreux, France, 1980).
[13]B. Combridge, J. Kripfganz, and J. Ranft, Phys. Lett. **70B**, 234 (1977); R. Cutler and D. Sivers, Phys. Rev. D **17**, 196 (1978).
[14]E. Argyres, A. P. Contogouris, M. Sanielevici, and H. Tanaka, Phys. Rev. D **29**, 2527 (1984). See also E. Berger, E. Braaten, and R. Field, Nucl. Phys. **B239**, 52 (1984).
[15]E. Berger, Phys. Rev. D **26**, 105 (1982).
[16]J. Owens, Phys. Rev. D **30**, 943 (1984).
[17]D. Duke and J. Owens, Phys. Rev. D **30**, 49 (1984).
[18]A. Nicolaidis, Nucl. Phys. **B163**, 156 (1980).
[19]H. Abramowicz *et al.* (CERN-Dortmund-Heidelberg-Saclay collaboration), Z. Phys. C **12**, 289 (1982); **17**, 283 (1983).
[20]A. Anassontzis *et al.*, Z. Phys. C **13**, 277 (1982); see also Fig. 17 of Ref. 1; L. Cormell and J. Owens, Phys. Rev. D **22**, 1609 (1980); O. Benary, E. Gotsman, and D. Lissauer, Z. Phys. C **16**, 211 (1983).
[21]P. Aurenche *et al.*, Phys. Lett. **140B**, 87 (1984).
[22]See also related discussion in Ref. 2. We have checked that these forms reproduce the $O(\alpha_s^2)$ corrections for $\pi^- p \to \gamma + X$ reported by D. Schiff, Report No. LPTHE Orsay 84/36 (unpublished).
[23]L. Beaulieu and C. Kounnas, Nucl. Phys. **B141**, 423 (1978); J. Kodaira and T. Uematsu, *ibid.* **B141**, 497 (1978).
[24]A. P. Contogouris and H. Tanaka, McGill report (unpublished).
[25]In Ref. 14 and elsewhere the value $C(qg \to \gamma q) = N - C_F$ has been used; this corresponds to a different definition of corrections (Ref. 24).
[26]G. Arnison *et al.* (UA1 collaboration), Phys. Lett. **136B**, 294 (1984).
[27]N. D. Antoniou, E. Argyres, A. P. Contogouris, M. Sanielevici, and S. D. P. Vlassopulos, Phys. Rev. D **29**, 1354 (1984); Phys. Lett. **128B**, 257 (1983).
[28]G. Donaldson *et al.*, Phys. Lett. **73B**, 375 (1978).
[29]J. Povlis *et al.*, Phys. Rev. Lett. **51**, 967 (1983).
[30]We would like to thank Professor M. Martin and Dr. M. Kienzle-Focacci for private communications.